Research article

Radiation shielding ability and optical features of La$_2$O$_3$+TiO$_2$+Nb$_2$O$_5$+WO$_3$+X$_2$O$_3$ (X=B, Ga, and In) glass system containing high-entropy oxides

Jamila S. Alzahrani [a], Z.A. Alrowaili [b], Canel Eke [c], Abeer S. Altowyan [a], I.O. Olarinoye [d], M.S. Al-Buriahi [e,*]

[a] *Department of Physics, College of Science, Princess Nourah bint Abdulrahman University, P.O. Box 84428, Riyadh 11671, Saudi Arabia*
[b] *Department of Physics, College of Science, Jouf University, P.O. Box 2014, Sakaka, Saudi Arabia*
[c] *Akdeniz University, Faculty of Education, Department of Mathematics and Science Education, Antalya, Turkey*
[d] *Department of Physics, School of Physical Sciences, Federal University of Technology, Minna, Nigeria*
[e] *Department of Physics, Sakarya University, Sakarya, Turkey*

ARTICLE INFO

ABSTRACT

Three high entropy materials (La$_2$O$_3$+TiO$_2$+Nb$_2$O$_5$+WO$_3$+X$_2$O$_3$ coded as LTNWM1, LTNWM2, and LTNWM3 for X = B, Ga, and In) produced by aerodynamic containerless processing were evaluated for optical attributes, and their gamma-radiation absorption abilities were investigated in this report. Optical related parameters such as the molar refractivity (R_m), optical transmission (T), molar polarizability (α_m), metallization criterion (M), reflection loss (R_L), static (ε^{static}), and optical ($\varepsilon^{optical}$) dielectric constants were estimated through standard expressions, while photon attenuation parameters were estimated from data from photon transmission simulations in FLUKA code and XCOM software. The attenuation parameters were calculated for a wide energy photon spectrum (15 keV–15 MeV). LTNWM1, LTNWM2, and LTNWM3 had R_m values of 18.94 cm^3/mol, 21.45 cm^3/mol, and 26.09 cm^3/mol respectively. The α_m has a value of 7.52 × 10^{-24} cm^3 for LTNWM1, 8.51 × 10^{-24} cm^3 for LTNWM2, and 10.35 × 10^{-24} cm^3 for LTNWM3. The photon shielding parameters evaluated by FLUKA and XCOM are compatible. The mass attenuation coefficient for the glasses was between 0.0338 and 52.8261 cm^2/g, 0.0336–58.0237 cm^2/g, and 0.0344–52.1560 cm^2/g for LTNWM1, LTNWM2 and LTNWM3, respectively. The effective atomic number at 1.5 MeV was 18.718, 20.857, and 22.440 for LTNWM1, LTNWM2, and LTNWM3, respectively. The shielding parameters of the HMOs compared to traditional gamma radiation absorbers are exceptional and highlight the potential of using them as optically transparent gamma-shields.

1. Introduction

The development of engineering materials in modern times is directly linked to economic and social development. Materials made from metals play a vital role in technological advancement and civilization. Therefore, the search for new metallic materials or methods of improving the attributes of existing ones by mixing different metals together are active areas of material science and

---

* Corresponding author.
E-mail address: mburiahi@gstd.sci.cu.edu.eg (M.S. Al-Buriahi).

development. This has led to the breaking of the limits of material properties and applications. High-entropy materials (HEMs) have the potential to break barriers in terms of the general features of engineering materials and, hence, the scope of applications. The HEMs are a grade of material classified based on their high entropy value and possess qualities that are unique [1]. Yeh et al. [2] and Cantor et al. [3] conducted the first research on HEMs concurrently, demonstrating that it is possible to obtain multicomponent alloys of nearly equal molar content, defined by a single phase, and solid solution structure, which could be implemented for various groups of materials such as alloys, nitrides, oxides, diborides, carbides, and silicides [4–12]. Then, Ross et al. demonstrated that the configurational irregularity could be utilized to obtain new oxide phases, enlarging the concept of high entropy alloys (HEAs) and introducing the concept of high entropy oxides (HEOs), which include five or more cations in an equimolar or near-equimolar mixture. Therefore, HEOs are similar to HEAs [13–15]. Recent studies have shown that HEOs have new features such as a colossal dielectric constant, narrow band gap, lithium superionic conductivity, and high temperature constancy [15–19]. HEMs have attractive qualities that make them the desirable materials in space, energy generation and harvesting, nuclear power, defense, robotics and many more applications. The search for more HEMs with exceptional attributes for emerging applications has since gained momentum.

The use of gamma-radiation for many peaceful purposes has persisted over the years due to the enormous benefits derived from its applications. Ionizing radiation is used for the destruction of harmful microorganisms (sterilization) in food, tools, and the environment; in medicine, different forms of radiation are used for diagnostic and therapeutic procedures; in research and industry, radiation is used for industrial radiography and material characterization, among other things. However, ionizing radiation is inherently dangerous when exposed to living tissues. In order to limit the adverse effects of gamma rays on living tissues and sensitive materials, the use of barriers known as shields to absorb radiation is often deployed together with other radiation protection principles. Emerging technology, knowledge of environmental conservation, durability, and other features have placed restrictions on the use of well-known shields such as concrete, lead (Pb), and lead-based composite materials for shielding applications. There has thus been a paradigm shift in the choice of materials employed in radiation shielding designs.

Composite materials such as alloys and glasses are attractive for shielding based on a couple of factors, among others. First, the mixture could be optimized to obtain desired properties such as mechanical, physical, and chemical features, which are required for a structural shield. Such optimization could also lead to exceptional properties that could make the materials stable in extreme radiation environments, such as in space or in a nuclear reactor facility. Second, composite materials can be designed in such a way that they contain different classes of atoms with a high probability of interactions with diverse radiation types. This is important in a mixed radiation field or in situations where the interaction of one form of radiation can give birth to another, such as in the radiative capture of neutrons. Therefore, composite materials, including glasses, rocks, and alloys, have been actively researched and recommended for radiation shielding in different radiation application scenarios [20–36]. Some of these materials have shown great potential as radiation shields; others have possessed certain qualities that make them preferable in different shielding scenarios. For instance, while composite materials such as bulk metallic glasses [22], marbles, granite [28], volcanic rocks [29], alloys [32], and concrete [34] have displayed good shielding attributes, their opaqueness has limited their applications in some medical and industrial applications of radiation where optical transparency of shields is advantageous. On the other hand, transparent glasses with good shielding abilities may lack the mechanical strength and temperature tolerance required in shielding materials for space exploration, nuclear power plants, and the construction of structural shields stable against other environmental factors. Availability, cost, and engineering workability are some of the factors that could limit the use of certain shielding materials in contemporary times. Therefore, the search for new shields with unique attributes useful in different application areas of ionizing radiation and environments is continuous. As the radiation application spectrum continues to expand, so too will the need to find novel materials with good shielding abilities and unique attributes for peculiar uses and environments.

As composite materials, HEMs, depending on their composition and associated properties, could be an important shield in many radiation-based technologies. Various properties of HEMs are being investigated by researchers with the objective of expanding the spectrum of attributes and potential applications. Radiation shielding properties are one area of emerging research on HEMs that has had sparse patronage so far. However, the limited available research on the radiation absorption capacity of some HEMs has produced encouraging results. For example, Zhang et al. [37] investigated experimentally the thermal neutron and gamma-ray shielding properties of the $(La_{0.2}Ce_{0.2}Gd_{0.2}Er_{0.2}Tm_{0.2})_2(WO_4)_3$ single-phase high-entropy ceramic material and concluded that this material has good gamma-ray shielding properties in both the low energy and medium energy regions. It is also convenient for thermal neutron and gamma-ray shielding. Sakar et al. [38] fabricated and studied the photon and particle attenuation characteristics of CoNiFeCr–Ti/Al high entropy alloys, and their results proved that the CoNiFeCr alloy had the greatest attenuation properties of the studied alloys and could be a suitable candidate for electron, photon, alpha, and neutron shielding applications. Gul et al. [39] examined the effects of B_4C on the structure, mechanical strength, and nuclear shielding capability of NiCoFeCrW high entropy alloys. The radiation shielding studies were conducted through experiments and theoretical methods. The results showed that the neutron attenuation properties of NiCoFeCrW high entropy alloys improve with increasing B_4C content, whereas there is no considerable variation in the gamma-ray absorption ability of the studied samples [39].

In this paper, the optical attributes of $20La_2O_3+20TiO_2+20Nb_2O_5+20WO_3+20B_2O_3$, $20La_2O_3+ 20TiO_2+ 20Nb_2O_5+ 20WO_3+ 20Ga_2O_3$, and $20La_2O_3 +20TiO_2 +20TiO_2+ 20Nb_2O_5+ 20WO_3+ 20In_2O_3$ high entropy oxide glasses were examined through the estimation of optical related parameters such as the molar refractivity (R_m), optical transmission (T), molar polarizability (α_m), metallization criterion (M), reflection loss (R_L), static (ε^{static}), and optical ($\varepsilon^{optical}$) dielectric constants. In addition, the gamma-photon shielding characteristics of the glasses are probed in order to ascertain their potential in radiation protection applications for the first time. According to a recently concluded study [40], these glasses show exceptional physical and optical features such as high density, mechanical strength, optical transparency in the visible region, and strong radiation resilience. These characteristics imply that the

glasses may be effective at gamma radiation absorption. Resilience to radiation is a strong attribute desired in a durable shielding material. As a result, these glasses may be suitable for the design of transparent structural shields. However, the role of B_2O_3, Ga_2O_3, and In_2O_3 in enhancing or otherwise the photon shielding ability of the HEMs is yet to be studied. In addition, the effectiveness of these materials in radiation shielding compared to standard shielding materials is required for proper recognition of their radiation attenuation potentials. Therefore, this study will improve existing scientific knowledge about these HMOs and expand their technological advantages and applications in optical and radiation shielding technologies.

2. Methodology

Three HEMs ($La_2O_3+TiO_2+Nb_2O_5+WO_3+X_2O_3$ coded as LTNWM1, LTNWM2, and LTNWM3 for X = B, Ga, and In) produced by aerodynamic containerless processing by Zhang et al. [40] were evaluated for optical attributes and gamma-radiation absorption abilities. The density and chemical structure of the HMOs are presented in Table 1 while further details about the preparation processes and radiation tolerance can be found in Ref. [40]. The following optical variables: R_m, α_m, R_L, T, M, ε^{static}, and $\varepsilon^{optical}$ were estimated through the standard formulae in Table 2 [41,42].

Parameters related to the gamma-radiation attenuation ability of the HMOs were estimated starting from the mass attenuation coefficient μ/ρ. The μ/ρ is a common parameter for discriminating the photon shielding abilities of materials. It can be estimated through gamma transmission experiments or Monte Carlo simulations with nearly equal accuracy or through definite online-software such as XCOM [43] and Phy-X/PSD [44] software. The use of Monte Carlo codes and the mentioned software are faster, more economical, radiologically safer, and more convenient ways of studying the radiation interaction parameters of different materials. Hence, a huge proportion of studies conducted through these theoretical approaches compared to experimental procedures. In the study, μ/ρ was estimated through a narrow photon beam transmission setup in the FLUKA Monte Carlo code. The geometry shown in Fig. 1 was adopted for the transmission simulations. The arrangement consists of a source of a single energy beam of photons, a sample, and a photon detector placed in the detector region (see Fig. 1). The thickness d (cm) of the sample and position were chosen such that the narrow beam transmission of photons was guaranteed. For the incident photon beam φ_i, HMO mass thickness of ρd (g/cm^2), and transmitted photon intensity φ_t, the μ/ρ was calculated based on the transmission equation given in Table 2 [22,24]. In addition, μ/ρ was calculated through the XCOM free platform for the materials. The calculations of μ/ρ in the simulations and direct calculations (XCOM) were for single photon energies within the range of 15 keV -15 MeV. As a way of understanding the photon interaction ability of the HMOs, other μ/ρ-dependent parameters such as the linear attenuation coefficient μ, effective atomic number Z_{eff}, mean-free path λ, and half-value layer HVL were estimated using the appropriate equation in Table 2 [22,24].

3. Results and discussion

3.1. Optical features

The values of R_m, α_m, R_L, T, M, ε^{static}, and $\varepsilon^{optical}$ of the studied HMO glasses are given in Table 3. Figs. 2 and 3 also show the plots of molar refractivity (R^{Mol}) (Fig. 2a), molar polarizability (α_m) (Fig. 2b), Optical loss (R^{Loss}) and optical transmission (T^{Opt}) (Fig. 3) of the glasses. The R_m, α_m, R_L, ε^{static}, and $\varepsilon^{optical}$ differ according to the order LTNWM1< LTNWM2< LTNWM3, while T and M follow a reverse trend. R_m is 18.94 cm^3/mol, 21.45 cm^3/mol, and 26.09 cm^3/mol for LTNWM1, LTNWM2, and LTNWM3 respectively. This shows that as X changes from B_2O_3 to Ga_2O_3 and In_2O_3 (see Tables 1 and 3), the glass network is more open and their molar volume increases. These increases could be due to the creation of non-bridging oxygen (NBO). The α_m has a value of 7.52×10^{-24} cm^3 for LTNWM1, 8.51×10^{-24} cm^3 for LTNWM2, and 10.35×10^{-24} cm^3 for LTNWM3. The polarizability of the X-oxides is believed to predict this observed trend. Furthermore, the increasing trend of the polarizability is as a result of the increase in the NBO relative to bridging oxygen (BO). Since NBO has higher α_m than BO [45], the introduction of Ga_2O_3 and In_2O_3 increases the NBO and makes LTNWM2 and LTNWM3 more polarized. The metallization criterion, M of LTNWM1, LTNWM2, and LTNWM3 had values of 0.456, 0.441, and 0.376, respectively. The metallization criterion is a measure of the insulating behavior of the materials. The M values of the investigated HEMs were all less than unity, thus, suggesting nonmetallic behavior. Based on the values, as X changes from B_2O_3 to Ga_2O_3 and In_2O_3, the insulating tendency of the HEMs increases. Fig. 3 shows the inverse relationship between the R_L and T of the samples. High surface reflection produces lower optical transmission; LTNWM3 has the highest reflectance loss (0.178) and the least optical transmittance (0.698) while LTNWM1 has the lowest R_L (0.132) and highest T (0.767). LTNWM1 has the highest M while LTNWM3 has the least (see Table 3 and Fig. 3). The values of the optical transmission show that the glasses are transparent in the visible spectrum and useful in areas where transparency is sought after.

Table 1
Chemical composition of the present investigated glassy samples.

Sample code	Chemical composition (mol. %)	Density (g/cm^3)
LTNWM1	$20La_2O_3$–$20TiO_2$–$20Nb_2O_5$–$20WO_3$–$20B_2O_3$	5.59
LTNWM2	$20La_2O_3$–$20TiO_2$–20 N Nb_2O_5–$20WO_3$–$20Ga_2O_3$	5.68
LTNWM3	$20La_2O_3$–$20TiO_2$–20 Nb_2O_5–$20WO_3$–$20In_2O_3$	5.83

Table 2
The equations for evaluating the optical parameters of the studied glass system.

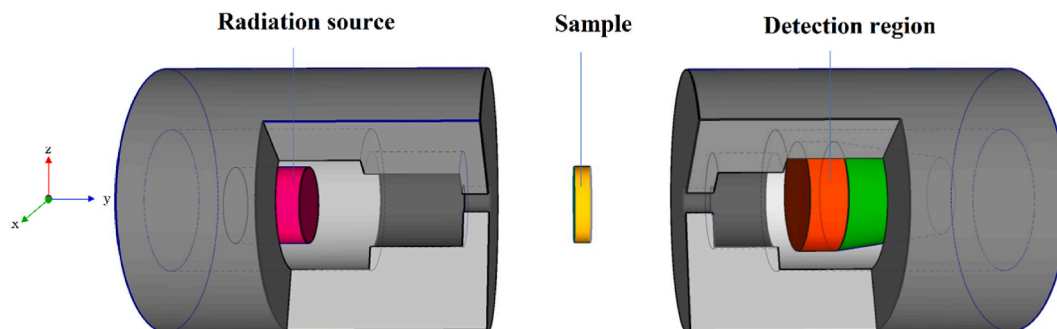| No.	Parameter	Equation
1	Molar refractivity, R_m (cm^3/mol)	$R_m = \left(\frac{n^2-1}{n^2+2}\right)V_{glass}$
2	Molar polarizability, $\alpha_m \times 10^{-24}$ cm^3	$\alpha_m = \frac{R_m}{2.52}$
3	Reflection loss, R_L	$R_L = \left(\frac{n-1}{n+1}\right)^2$
4	Optical transmission, T	$T = \frac{2n}{n^2+1}$
5	Metallization criterion, M	$M(n) = 1 - \left(\frac{n^2-1}{n^2+2}\right)$
6	Static dielectric constant, ε^{static}	$\varepsilon^{static} = n^2$
7	Optical dielectric constant, $\varepsilon^{optical}$	$\varepsilon^{optical} = \varepsilon^{static}-1$
8	Mass attenuation coefficient, μ/ρ (cm^2/g)	$\mu/\rho = \ln\left(\frac{\varphi_i}{\varphi_t}\right)\Big/ \rho d$
9	Linear attenuation coefficient, μ (cm^{-1})	$\mu = \mu/\rho\left(\frac{cm^2}{g}\right) \times \rho\left(\frac{g}{cm^3}\right)$
10	Effective atomic number, Z_{eff}	$Z_{eff} = \frac{\sum_i f_i A_i (\mu/\rho)_i}{\sum_i f_j \frac{A_i}{Z_i}(\mu/\rho)_i}$
11	Mean free path, λ (cm)	$\lambda = 1/\mu$
12	Half-value layer, $d_{1/2}$ (cm)	$d_{1/2} = \frac{ln\,2}{\mu}$

Fig. 1. Monte Carlo setup in the present work by using FLUKA simulations.

Table 3
Optical properties such as R_m, α_m, R_L, T, M, ε^{static}, and $\varepsilon^{optical}$ of the studied glasses.

Optical property/glass code	LTNWM1	LTNWM2	LTNWM3
Molar volume, Vm (cm3/mol)	34.811	38.408	41.584
Molar refractivity, R_m (cm^3/mol)	18.939	21.454	26.090
Molar polarizability, $\alpha_m \times 10^{-24}$ cm^3	7.515	8.513	10.353
Reflection loss, R_L	0.132	0.139	0.178
Optical transmission, T	0.767	0.756	0.698
Metallization criterion, M	0.456	0.441	0.373
Static dielectric constant, ε^{static}	4.580	4.796	6.052
Optical dielectric constant, $\varepsilon^{optical}$	3.580	3.796	5.052

3.2. Gamma-shielding variables

The μ/ρ of LTNWM glasses obtained from simulation techniques and XCOM are tabulated in Table 4. The two sets of data agree well with one another based on the values of the deviations Dev. (in %) between them (also shown in the table). The Dev. Generally changes between 0.01 and 1.80% for the three materials and investigated energy range. The agreement between FLUKA and XCOM generated μ/ρ indicates that the simulation was conducted in an approximately narrow beam geometry. The value of the μ/ρ differ for each glass at each energy level indicates an energy and chemical composition influence on μ/ρ. The mass attenuation coefficient for the glasses is
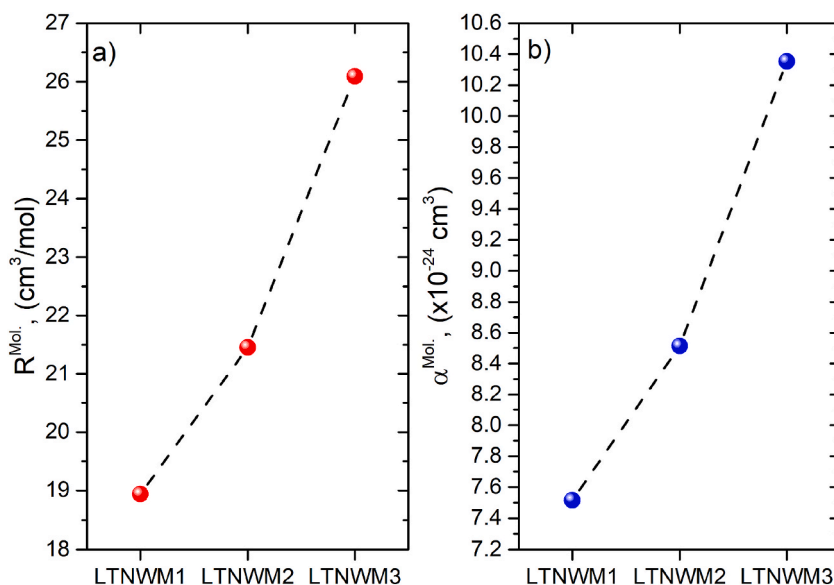
Fig. 2. Optical properties of the present investigated glassy samples (a) Molar refractivity (R^{Mol}) and (b) Molar polarizability (α_m).
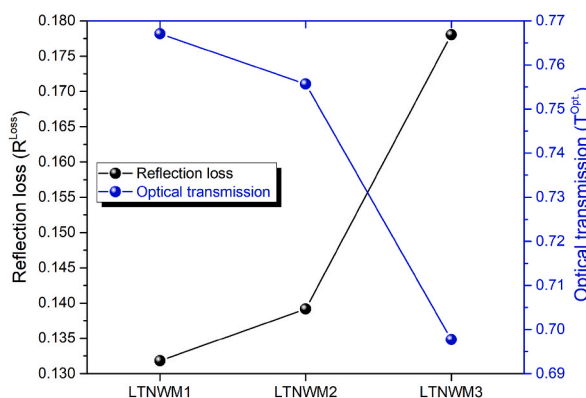

Fig. 3. Optical loss (R^{Loss}) and optical transmission (T^{Opt}) of the present investigated glassy samples).

maximum at 0.015 MeV with corresponding values of 52.8261 cm²/g, 58.0237 cm²/g and 52.1560 cm²/g for LTNWM1, LTNWM2 and LTNWM3. Minimum values of 0.0338 cm²/g, 0.0336 cm²/g and 0.0344 cm²/g were recorded at 6 MeV for LTNWM1, LTNWM2 and LTNWM3, respectively. To further analyze the energy and compositional-induced changes in the attenuation coefficient, the μ is plotted against energy in Fig. 4. The μ of the studied glasses falls within the interval 0.189–295.298 cm^{-1} for LTNWM1, 0.191–329.575 cm^{-1} for LTNWM2 and 0.195–296.246 cm^{-1} for LTNWM3. The attenuation coefficients consistently decrease with energy up to 6 MeV and then increase slightly for the rest of the investigated gamma-ray energies. In contrast to one another, it appears there are no considerable differences between the μ of studied glasses. This could be due to the similar composition of the glasses; hence, substituting B_2O_3 for Ga_2O_3 and In_2O_3 does not produce conspicuous changes in the linear and mass attenuation coefficients. This could also be because, the substitutions narrowly change the weight fraction of W (the element with the highest cross section for photons) between 16 and 19%. Perhaps the attenuation coefficient of W plays a key role in delineating the photon absorbing patterns of the HEMs. However, the energy variations of the attenuation coefficients are dictated by the photoelectric, Compton scattering, and pair production absorption cross-sections and their energy responses [22,24]. Both the photoelectric and pair production absorption processes completely absorb photons, while Compton scattering reduces the energy and penetration powers of photons through incoherent scattering. Therefore, attenuation coefficients are high where the former two processes dominate and low where the latter is significant. High but rapidly declining values of attenuation coefficients is believed to be caused by the photoelectric process, whose probability decreases inversely with at least the third power of the photon energy. Between 0.8 and 6 MeV, the Compton scattering dominates the interactions of photons with the HEMs, hence, the low value of the linear and mass attenuation coefficients. Also, within this energy range, the decrease in the values of the attenuation factor is slower due to the cross-section of incoherent scattering varying inversely with energy raised to a power of unity. Due to pair production effects, the attenuation coefficients of the investigated

Table 4
Mass attenuation coefficient (μ/ρ) (cm^2/g) of the LTNWM1, LTNWM2, and LTNWM3 glasses obtained by FLUKA Monte Carlo and XCOM program with different photons energies.

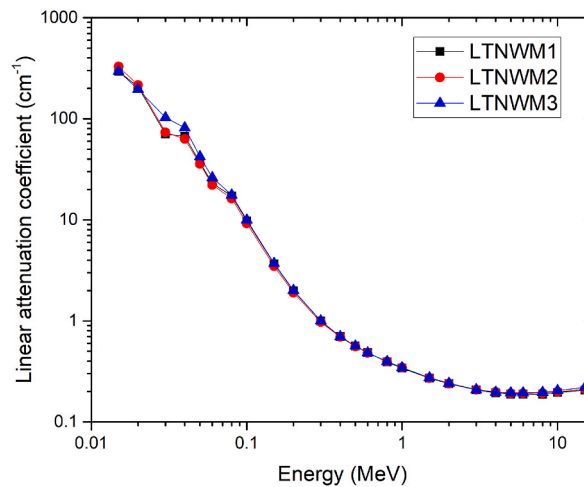| Photon Energy (MeV)	LTNWM1			LTNWM2			LTNWM3		
	XCOM	FLUKA	Dev.%	XCOM	FLUKA	Dev.%	XCOM	FLUKA	Dev.%
0.015	52.826	52.656	0.32	58.024	57.805	0.38	52.156	51.970	0.36
0.02	37.060	37.022	0.10	38.072	38.035	0.10	34.501	34.456	0.13
0.03	12.738	12.587	1.19	12.996	12.931	0.50	18.169	18.052	0.64
0.04	11.896	11.955	0.50	11.339	11.077	2.32	13.439	14.401	7.16
0.05	6.645	6.619	0.39	6.317	6.290	0.42	7.475	7.436	0.52
0.06	4.122	4.108	0.34	3.912	3.902	0.26	4.619	4.609	0.22
0.08	3.089	3.091	0.07	2.865	2.869	0.11	3.108	3.107	0.02
0.1	1.755	1.752	0.18	1.629	1.626	0.19	1.756	1.754	0.11
0.15	0.658	0.655	0.35	0.615	0.613	0.24	0.654	0.651	0.34
0.2	0.356	0.354	0.37	0.336	0.335	0.20	0.352	0.352	0.05
0.3	0.179	0.178	0.21	0.172	0.171	0.24	0.177	0.176	0.23
0.4	0.125	0.125	0.08	0.122	0.122	0.36	0.124	0.123	0.26
0.5	0.101	0.100	0.32	0.099	0.098	0.29	0.100	0.100	0.01
0.6	0.087	0.087	0.39	0.085	0.085	0.54	0.086	0.085	0.86
0.8	0.071	0.070	0.74	0.070	0.070	0.41	0.070	0.070	0.63
1	0.061	0.061	0.95	0.061	0.061	0.47	0.061	0.061	0.56
1.5	0.049	0.049	0.56	0.049	0.048	1.39	0.048	0.048	0.54
2	0.043	0.043	0.34	0.043	0.042	0.84	0.043	0.043	0.18
3	0.037	0.037	0.70	0.037	0.037	1.32	0.037	0.037	1.50
4	0.035	0.035	1.07	0.035	0.035	0.25	0.035	0.035	1.80
5	0.034	0.034	1.33	0.034	0.034	0.80	0.035	0.034	1.41
6	0.034	0.034	0.13	0.034	0.034	0.23	0.034	0.034	0.55
8	0.034	0.033	1.73	0.034	0.034	0.07	0.035	0.035	1.23
10	0.035	0.035	0.22	0.035	0.035	0.64	0.036	0.036	0.01
15	0.037	0.037	1.51	0.037	0.037	0.69	0.039	0.039	0.73

Fig. 4. Linear attenuation coefficient of the present investigated glassy samples.

materials begin to rise slowly for energies above 6 MeV.

The Z_{eff} is a gamma-ray interaction variable used in radiation physics to characterize a material's energy absorption ability and also to find material equivalence in terms of gamma-interaction responses and attenuation. Its value depends on the photon energy and the range of atomic number Z of the constituents of a composite material. The effective Z is more sensitive to changes in the chemical composition of a composite material and the incident photon energy. Therefore, it is a better parameter for delineating the difference in the photon energy absorption or attenuation efficiency of different interacting media. The Z_{eff} changes within the studied photon energies is shown in Fig. 5. Values of Z_{eff} are lowest at 1.5 MeV with values of 18.718, 20.857 and 22.440 for LTNWM1, LTNWM2 and LTNWM3, respectively, and maximal at 0.015 MeV with values of 55.073 and 54.054 for LTNWM1 and LTNWM2, respectively. The Z_{eff} value of LTNWM2 is maximum at 0.08 MeV with a value of 53.540. The K-absorption edges of W (0.07 MeV) and La (0.04 MeV) are believed to be responsible for the strong vibration in the values at the lower energy end of the spectrum. Generally, Z_{eff} decreases form maximum to lowest values at 1.5 MeV then they increase gradually up to 15 MeV as shown in Fig. 5. The photoelectric process, and the Compton scattering are responsible for the higher but decreasing values of Z_{eff} at energies less than 1.5 MeV. The pair production
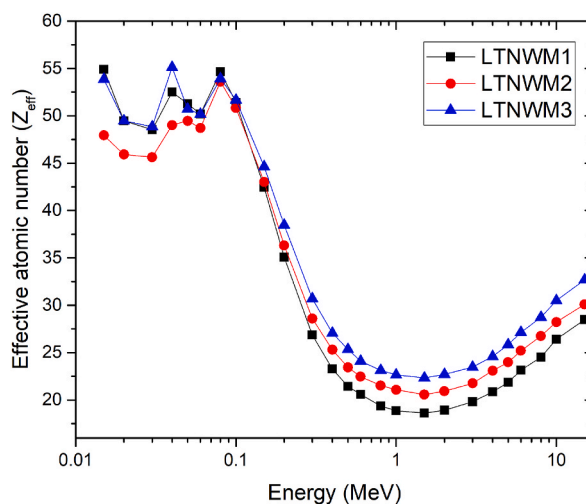
Fig. 5. Effective atomic number of the present investigated glassy samples.

effect, however, is responsible for the slight increase in the effective Z at greater energies. For most of the energy spectrum, the effective Z follows the pattern: LTNWM1< LTNWM2< LTNWM3. This is precipitated by the limits of the Z of the constituent atoms. The fact that the Z of B < Ga < In contributes largely to the trend of the Z_{eff}. The distinct differences in the Z_{eff} is an indication that the three glasses cannot be used as a substitutes of the same materials in radiation studies. Furthermore, LTNWM3 absorbs more photons and photon energy the most among the three materials while, LTNWM1 absorbs photon the least.

The mean free paths (λ) of studied glasses vary from 0.0034 cm to 5.2965 cm for LTNWM1, from 0.0030 cm to 5.2330 cm for LTNWM2, and from 0.0034 cm to 5.1168 cm for LTNWM. The λ of the LTNWM glasses is least at 0.015 MeV and highest at 6 MeV (see Fig. 6). After 6 MeV, the λ tend to be decline up to 15 MeV. The increase or decrease in the value of λ indicates decreasing or increasing photon interactions, respectively. Fig. 6 thus shows that the ability of the glasses to absorb photons declines as the gamma-photon energy increases. In agreement with other evaluated parameters, the relative photon shielding efficiency is dictated by the fact that the Z of B < Ga < In.

In practical scenarios, shielding requirements are presented in thickness units. The half-value layer ($d_{1/2}$) is the thickness of a shield needed to reduce a photon flux defined by its energy by 50%. Using $d_{1/2}$ is more convenient in shielding designs and implementations as it can be used to estimate the thickness required to absorb a specific proportion of a single enegy beam of photons. The $d_{1/2}$ of the present HMOs are within the intervals of 0.0023–3.6712 cm for LTNWM1, 0.0021–3.6373 cm for LTNWM2 and 0.0023–3.5467 cm for LTNWM3. The $d_{1/2}$ changes with energy in a similar way with λ. In Fig. 7, $d_{1/2}$ at 1 and 10 MeV was compared for the glasses. At 1 MeV photon energy, the $d_{1/2}$ of studied glasses are about 2 cm and at 10 MeV photon energy, the $d_{1/2}$ of studied glasses falls within 3.54–3.67 cm. At 10 MeV photon energy, the $d_{1/2}$ of LTNWM1 is the highest, while the HVLs of LTNWM3 is the least. This implies that at 10 MeV, LTNWM3 is a better photon absorber compared to LTNWM1 and LTNWM2. Compared to ordinary concrete (OC) [46], VR3 volcanic rock [47], commercial RS-253 & RS-360 glasses [48,49], and MASLN4 [50] with respective value of 12.61 cm, 9.43 cm, 11.89 cm, 4.66 cm, and 11.67 cm for $d_{1/2}$ at 10 MeV, LTNWM1, LTNWM2, and LTNWM3 are exceptional photon shields. Also, Table 5 compares the mass attenuation coefficient of the HEMs with previously researched and standard shielding materials for 0.511 MeV. Clearly, the HEMs are better than OC, Cu0·2Ag0.8 alloy, Ni-based alloy, and Fe-based alloy. The LTNWMX have advantage compared to better shields such as PB20, Pb-based alloy, and RS-%20 glass in that it does not contain Pb and lighter. The shielding ability of the present materials can be further improved by increasing their thickness in practical shielding designs.

4. Conclusion

The optical and gamma-shielding parameters of three HMOs, LTNWM1, LTNWM2, and LTNWM3 were theoretically estimated in order to evaluate their functionality in the optical and radiation protection fields. The estimated optical parameters of the glasses are distinct, varying according to the composition of the glasses. The molar refractivity values was 18.94 cm^3/mol, 21.45 cm^3/mol, and 26.09 cm^3/mol for LTNWM1, LTNWM2, and LTNWM3 respectively. The optical transmission of the glasses varies as well, but was above 0.69 for the three glasses. The optical constants of the glasses show that they are suitable for optical applications. The mass attenuation coefficients of the glasses evaluated through FLUKA simulations and XCOM software were in good agreement. The mass attenuation 0.0338–52.8261 cm^2/g, 0.0336–58.0237 cm^2/g and 0.0344–52.1560 cm^2/g for LTNWM1, LTNWM2 and LTNWM3. Also, for most of the energy spectrum, the effective Z follows the pattern: LTNWM1< LTNWM2< LTNWM3. The investigated HMOs have higher shielding effectiveness compared to some conventional shielding materials. The investigated glasses have useful attributes that can be exploited in optical and radiation safety technologies. They can be used as transparent gamma shields in medical applications of radiation, unlike opaque shields like Pb, rocks, alloys, and different concrete categories. The present materials are made from metals,
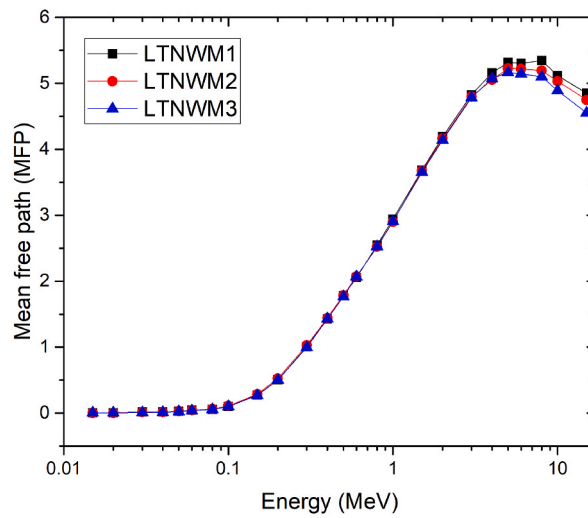
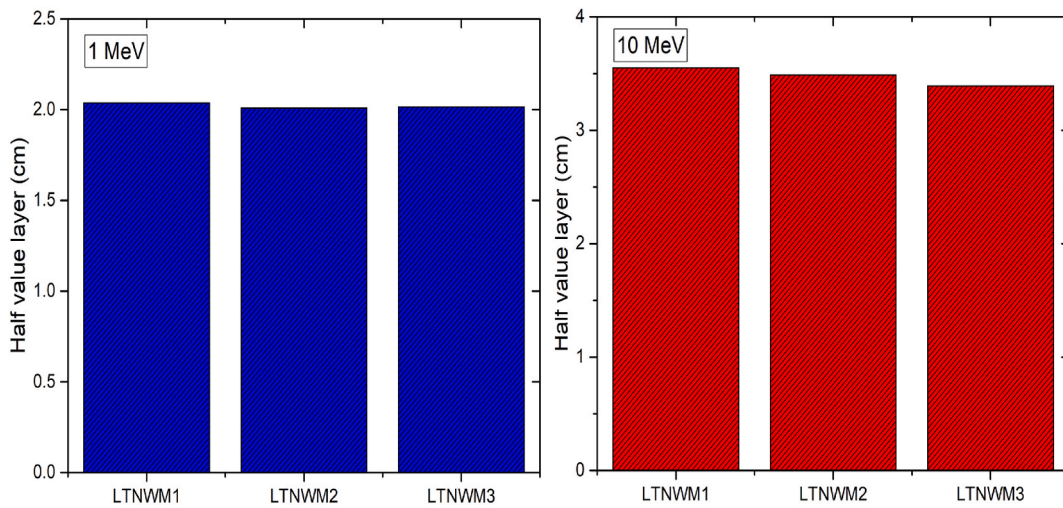**Fig. 6.** Mean free path of the present investigated glassy samples.

Fig. 7. Half value layer of the present investigated glassy samples at 1 MeV and 10 MeV.

Table 5
Comparison of mass attenuation coefficient of present HEMs with previous and standard shielding materials for 0.511 MeV photons.

Material	Nature of Material	Mass attenuation coefficient (cm^2g^{-1})	References
LTNWM1	HEM	0.1010	This study
LTNWM2	HEM	0.0987	This study
LTNWM3	HEM	0.0997	This study
PB20	Ceramics	0.1140	[30]
Cu0·2Ag0.8	Alloy	0.0896	[32]
Ni-alloy	Ni-based alloy	0.0868	[33]
Fe-alloy	Fe-based alloy	0.0833	[33]
Pb-alloy	Pb-based alloy	0.1500	[33]
W-alloy	W-based alloy	0.1330	[33]
OC	Ordinary concrete	0.0891	[51]
RS360	Glass	0.1150	[40,41]
R520	Glass	0.1320	[40,41]

which suggests they are mechanically stronger, more durable, and more rugged. Being dense materials, the quantity or thickness required for constructing a shield is reduced (especially within the medical diagnostic range), which makes the shielding design simple and less elaborate.

Author contribution statement

Jamila S. Alzahrani, Chalermpon Mutuwong: Conceived and designed the experiments; Performed the experiments; Wrote the paper.

Canel Eke, Abeer S. Altowyan: Analyzed and interpreted the data; Wrote the paper.

I.O. Olarinoye, M.S. Al-Buriahi: Contributed reagents, materials, analysis tools or data; Wrote the paper.

Acknowledgement

Data availability statement

No data was used for the research described in the article.

Declaration of interest's statement

The authors declare that they have no known competing financial interests or personal relationships that could have appeared to influence the work reported in this paper.

References

[1] P.K. Liaw, W. Li, High entropy materials: challenges and prospects, Metals 11 (2021) 1643, https://doi.org/10.3390/met11101643.

[2] J.W. Yeh, S.K. Chen, S.J. Lin, J.Y. Gan, T.S. Chin, T.T. Shun, et al., Nanostructured high-entropy alloys with multiple principal elements: novel alloy design concepts and outcomes, Adv. Eng. Mater. 6 (5) (2004) 299–303, https://doi.org/10.1002/adem.20030056.

[3] B. Cantor, I.T.H. Chang, P. Knight, A.J.B. Vincent, Microstructural development in equiatomic multicomponent alloys, Mater. Sci. Eng., A 375–377 (2004) 213–218, https://doi.org/10.1016/j.msea.2003.10.257.

[4] K.M. Katubi, R. Kurtulus, Z.A. Alrowaili, T. Kavas, E. Kavaz, M.S. Al-Buriahi, Optical properties, elastic moduli, and radiation shielding performance of some waste glass systems treated by bismuth oxide, Optik 266 (2022) 169567.

[5] Z. Grzesik, G. Smoła, M. Miszczak, M. Stygar, J. Dąbrowa, M. Zajusz, K. Świerczek, M. Danielewski, Defect structure and transport properties of (Co,Cr,Fe,Mn, Ni)$_3$O$_4$ spinel-structured high entropy oxide, J. Eur. Ceram. Soc. 40 (2019) 835–839, https://doi.org/10.1016/j.jeurceramsoc.2019.10.026.

[6] Y. Zhang, T.T. Zuo, Z. Tang, M.C. Gao, K.A. Dahmen, P.K. Liaw, Z.P. Lu, Microstructures and properties of high-entropy alloys, Prog. Mater. Sci. 61 (2014) 1–93, https://doi.org/10.1016/j.pmatsci.2013.10.001.

[7] S.Y. Chang, M.K. Chen, D.S. Chen, Multiprincipal-element AlCrTaTiZr-nitride nanocomposite film of extremely high thermal stability as diffusion barrier for Cu metallization, J. Electrochem. Soc. 156 (5) (2009) G37–G42.

[8] Y. Long, J. Che, Z. Wu, H.-T. Lin, F. Zhang, High entropy alloy borides prepared by powder metallurgy process and the enhanced fracture toughness by addition of yttrium, Mater. Chem. Phys. 257 (2021), 123715, https://doi.org/10.1016/j.matchemphys.2020.123715.

[9] J. Zhou, J. Zhang, F. Zhang, B. Niu, L. Lei, W. Wang, High-entropy carbide: a novel class of multicomponent ceramics, Ceram. Int. 44 (2018) 22014–22018, https://doi.org/10.1016/j.ceramint.2018.08.100.

[10] B. Ye, T. Wen, Y. Chu, High-temperature oxidation behavior of (Hf0.2Zr0.2Ta0.2Nb0.2Ti0.2)C high-entropy ceramics in air, J. Am. Ceram. Soc. 103 (2019) 500–507, https://doi.org/10.1111/jace.16725.

[11] J. Gild, J. Braun, K. Kaufmann, E. Marin, T. Harrington, P. Hopkins, K. Vecchio, J. Luo, A high-entropy silicide: (Mo0.2Nb0.2Ta0.2Ti0.2W0.2)Si2, J. Materiomics 5 (2019) 337–343, https://doi.org/10.1016/j.jmat.2019.03.002.

[12] A.L. Vyatskikh, B.E. MacDonald, A.D. Dupuy, E.J. Lavernia, J.M. Schoenung, H. Hahn, High entropy silicides: CALPHAD-guided prediction and thin film fabrication, Scripta Mater. 201 (2021), 113914, https://doi.org/10.1016/j.scriptamat.2021.113914.

[13] C.M. Rost, E. Sachet, T. Borman, A. Moballegh, E.C. Dickey, D. Hou, J.L. Jones, S. Curtarolo, J.-P. Maria, Entropy-stabilized oxides, Nat. Commun. 6 (2015) 8485, https://doi.org/10.1038/ncomms9485.

[14] D. Berardan, A.K. Meena, S. Franger, C. Herrero, N. Dragoe, Controlled Jahn-Teller distortion in (MgCoNiCuZn)O-based high entropy oxides, J. Alloys Compd. 704 (2017) 693–700, https://doi.org/10.1016/j.jallcom.2017.02.070.

[15] M.R. Chellali, A. Sarkar, S.H. Nandam, S.S. Bhattacharya, B. Breitung, H. Hahn, L. Velasco, On the homogeneity of high entropy oxides: an investigation at the atomic scale, Scripta Mater. 166 (2019) 58–63, https://doi.org/10.1016/j.scriptamat.2019.02.039.

[16] D. Bérardan, S. Franger, D. Dragoe, A.K. Meena, N. Dragoe, Colossal dielectric constant in high entropy oxides, Phys. Status Solidi Rapid Res. Lett. 10 (4) (2016) 328–333, https://doi.org/10.1002/pssr.201600043.

[17] B. Xiao, G. Wu, T. Wang, Z. Wei, Y. Sui, B. Shen, J. Qi, F. Wei, J. Zheng, High-entropy oxides as advanced anode materials for long-life lithium-ion Batteries, Nano Energy 95 (2021), 106962, https://doi.org/10.1016/j.nanoen.2022.106962.

[18] D. Bérardan, S. Franger, A.K. Meena, N. Dragoe, Room temperature lithium superionic conductivity in high entropy oxides, J. Mater. Chem. A 4 (2016) (2016) 9536–9541, https://doi.org/10.1039/C6TA03249D.

[19] J. Sun, L. Guo, Y. Zhanh, Y. Wang, K. Fan, Y. Tang, Superior phase stability of high entropy oxide ceramic in a wide temperature range, J. Eur. Ceram. Soc. 42 (2022) 5053–5064, https://doi.org/10.1016/j.jeurceramsoc.2022.05.007.

[20] M.S. Al-Buriahi, Z.A. Alrowaili, S. Alomairy, I.O. Olarinoye, C. Mutuwong, Optical properties and radiation shielding competence of Bi/Te-BGe glass system containing B2O3 and GeO2, Optik 257 (2022), 168883, https://doi.org/10.1016/j.ijleo.2022.168883.

[21] I.O. Olarinoye, S. Alomairy, C. Sriwunkum, H.H. Hegazy, M.S. Al-Buriahi, Effects of TeO2 and B2O3 on photon, neutron, and charged particle transmission properties of Bi2O3-BaO-LiF glass system, Journal of the Australian Ceramic Society 57 (4) (2021) 1177–1188, https://doi.org/10.1007/s41779-021-00616-y.

[22] Katubi, Khadijah Mohammedsaleh, Imen Kebaili, Z.A. Alrowaili, Canel Eke, I.O. Olarinoye, M.S. Al-Buriahi, Gamma shielding performance of the optical B2O3-based glass system, Optik 270 (2022), 169914.

[23] Katubi, Khadijah Mohammedsaleh, Canel Eke, Norah Alwadai, Z.A. Alrowaili, Chalermpon Mutuwong, M.S. Al-Buriahi, Influence of Fe2O3 content on the optical features and radiation shielding efficiency of CaO-Na2O-B2O3 glass system, Optik 265 (2022), 169473.

[24] Katubi, Khadijah Mohammedsaleh, Awad A. Ibraheem, Norah Alwadai, Z.A. Alrowaili, I.O. Olarinoye, Chahkrit Sriwunkum, M.S. Al-Buriahi, Enhancement on radiation shielding performance of B2O3+ Li2O+ ZnO+ Na2O glass system, Radiat. Phys. Chem. 201 (2022), 110457.

[25] Katubi, Khadijah Mohammedsaleh, I.O. Olarinoye, Z.A. Alrowaili, M.S. Al-Buriahi, Optical transmission, polarizability, and photon/neutron shielding properties of Bi2O3/MnO/B2O3 glass system, Optik 268 (2022), 169695.

[26] R. Kurtulus, G.A. Alharshan, T. Kavas, E. Kavaz, I. Kebaili, I.O. Olarinoye, M.S. Al Buriahi, Recycling potential of mobile phone waste glasses for radiation shielding applications, Radiat. Phys. Chem. 110565 (2022), https://doi.org/10.1016/j.radphyschem.2022.110565.

[27] Katubi, Khadijah Mohammedsaleh, Recep Kurtulus, Z.A. Alrowaili, Taner Kavas, E. Kavaz, M.S. Al-Buriahi, Optical properties, elastic moduli, and radiation shielding performance of some waste glass systems treated by bismuth oxide, Optik 266 (2022), 169567.

[28] Olarinoye, I. O., Siraju, K. O., & AA, A. Assessment of Shielding Potentials and Radiological Safety Indices of Nigerian Granite Rocks. https://dx.doi.org/10.4314/njtr.v14i2.11.

[29] A. Saeed, S. Alomairy, C. Sriwunkum, M.S. Al-Buriahi, Neutron and charged particle attenuation properties of volcanic rocks, Radiat. Phys. Chem. 184 (2021), 109454, https://doi.org/10.1016/j.radphyschem.2021.109454.

[30] A.H. Almuqrin, A. Kumar, J.F.M. Jecong, N. Al-Harbi, E. Hannachi, M.I. Sayyed, Li2O-K2O-B2O3-PbO glass system: optical and gamma-ray shielding investigations, Optik 247 (2021), 167792.

[31] E. Hannachi, K.A. Mahmoud, M.I. Sayyed, Y. Slimani, Structure, optical properties, and ionizing radiation shielding performance using Monte Carlo simulation for lead-free BTO perovskite ceramics doped with ZnO, SiO2, and WO3 oxides, Mater. Sci. Semicond. Process. 145 (2022), 106629.

[32] M.F. Turhan, F. Akman, A. Taşer, K. Dilsiz, H. Oğul, M.R. Kacal, O. Agar, Gamma radiation shielding performance of CuxAg (1-x)-alloys: experimental, theoretical and simulation results, Prog. Nucl. Energy 143 (2022), 104036.

[33] J.S. Alzahrani, Z.A. Alrowaili, C. Eke, Z.M. Mahmoud, C. Mutuwong, M.S. Al-Buriahi, Nuclear shielding properties of Ni-, Fe-, Pb-, and W-based alloys, Radiat. Phys. Chem. 195 (2022), 110090.

[34] M.A.H. Abdullah, R.S.M. Rashid, M. Amran, F. Hejazii, N.M. Azreen, R. Fediuk, M.I. Idris, Recent trends in advanced radiation shielding concrete for construction of facilities: materials and properties, Polymers 14 (14) (2022) 2830.

[35] E. Hannachi, K.A. Mahmoud, A.H. Almuqrin, M.I. Sayyed, Y. Slimani, Evaluation of the radiation-protective properties of Bi (Pb)–Sr–Ca–Cu–O ceramic prepared at different temperatures with silver inclusion, Materials 15 (3) (2022) 1034.

[36] M.I. Sayyed, E. Hannachi, K.A. Mahmoud, Y. Slimani, Synthesis of different (RE) BaCuO ceramics, study their structural properties, and tracking their radiation protection efficiency using Monte Carlo simulation, Mater. Chem. Phys. 276 (2022), 125412.

[37] X. Zhang, Y. Li, C. Li, F. Yang, Z. Jiang, L. Xue, Z. Shao, Z. Zhao, M. Xie, S. Yu, A novel (La0.2Ce0.2Gd0.2Er0.2Tm0.2)2(WO4)3 high-entropy ceramic material for thermal neutron and gamma-ray shielding, Mater. Des. 205 (2021), 109722, https://doi.org/10.1016/j.matdes.2021.109722.

[38] Alzahrani, S. Jamila, Z.A. Alrowaili, H.H. Saleh, Alaa Hammoud, Sultan Alomairy, C. Sriwunkum, Synthesis, physical and nuclear shielding properties of novel Pb–Al alloys, Progress Nuclear Energy 142 (2021), 103992.

[39] A.O. Gul, E. Kavaz, O. Basgoz, O. Guler, G. Alminsed, E. Bahceci, M.G. Albayrak, H.O. Tekin, Newly synthesized NiCoFeCrW High-Entropy Alloys (HEAs): multiple impacts of B4C additive on structural, mechanical, and nuclear shielding properties, Intermetallics 146 (2022), 107593, https://doi.org/10.1016/j.intermet.2022.107593.

[40] X. Zhang, J. Zhang, C. Zhou, L. Li, X. Qi, Optical properties and irradiation resistance of novel high-entropy oxide glasses La2O3–TiO2–Nb2O5–WO3–M2O3 (M= B/Ga/In), J.Rare Earths. (2022).

[41] K.M. Kaky, M.I. Sayyed, A. Khammas, A. Kumar, E. Şakar, A.H. Abdalsalam, M.H.A. Mhareb, Theoretical and experimental validation gamma shielding properties of B2O3–ZnO–MgO–Bi2O3 glass system, Mater. Chem. Phys. 242 (2020), 122504, https://doi.org/10.1016/j.matchemphys.2019.122504.

[42] M.S. Al-Buriahi, C. Eke, Z.A. Alrowaili, A.M. Al-Baradi, I. Kebaili, B.T. Tonguc, Optical properties and radiation shielding performance of tellurite glasses containing Li2O and MoO3, Optik 249 (2022), 168257, https://doi.org/10.1016/j.ijleo.2021.168257.

[43] M.J. Berger, J.H. Hubbell, XCOM: Photon Cross Sections on a Personal Computer (No. NBSIR-87-3597). National Bureau of Standards, Center for Radiation Research, Washington, DC (USA), 1987, https://doi.org/10.2172/6016002.

[44] E. Şakar, Ö.F. Özpolat, B. Alım, M.I. Sayyed, M. Kurudirek, Phy-X/PSD: development of a user friendly online software for calculation of parameters relevant to radiation shielding and dosimetry, Radiat. Phys. Chem. 166 (2020), 108496, https://doi.org/10.1016/j.radphyschem.2019.108496.

[45] M.N. Azlan, M.K. Halimah, S.Z. Shafinas, W.M. Daud, Electronic polarizability of zinc borotellurite glass system containing erbium nanoparticles, Materials Express 5 (3) (2015) 211–218.

[46] I.I. Bashter, Calculation of radiation attenuation coefficients for shielding concretes, Ann. Nucl. Energy 24 (17) (1997) 1389–1401, https://doi.org/10.1016/S0306-4549(97)00003-0.

[47] A. Saeed, S. Alomairy, C. Sriwunkum, M.S. Al-Buriahi, Neutron and charged particle attenuation properties of volcanic rocks, Radiat. Phys. Chem. 184 (2021), 109454, https://doi.org/10.1016/j.radphyschem.2021.109454.

[48] Speit, B. Radiation-shielding glasses providing safety against electrical discharge and being resistant to discoloration, U.S. Patent 5,073,524, issued December 17, 1991.

[49] https://www.schott.com/en-ca/products/radiation-shielding-glasses/product-variants?tab=rs-glass-series. (Accessed 22 January 2022). Accessed.

[50] M.A. Alothman, I.O. Olarinoye, C. Sriwunkum, S. Alomairy, J.S. Alzahrani, M.S. Al-Buriahi, Study of the radiation attenuation properties of MgO-Al2O3-SiO2-Li2O-Na2O glass system, J. Australas. Ceram. Soc. (2021), https://doi.org/10.1007/s41779-021-00687-x.

[51] https://physics.nist.gov/PhysRefData/XrayMassCoef/ComTab/concrete.html. Accessed on 29th December, 2022.